

## The *Large Area Telescope* on the *GLAST* Mission

Authors: Category 1 paper

### ABSTRACT

The Large Area Telescope (LAT), one of two instruments on the Gamma-ray Large Area Space Telescope (GLAST) mission, scheduled for launch by NASA in 2007, is an imaging, wide field-of-view, high-energy gamma-ray telescope, covering the approximate energy range from 20 MeV to more than 300 GeV. The LAT is being built by an international collaboration with contributions from space agencies, high-energy particle physics institutes, and universities in France, Italy, Japan, Sweden and the United States. The scientific objectives the LAT will address include (1) resolving the high-energy gamma-ray sky and determining the nature of the unidentified gamma-ray sources seen by EGRET and the origin of the apparently isotropic diffuse emission, (2) understanding the mechanisms of particle acceleration in celestial sources, including active galactic nuclei, pulsars, and supernovae remnants, (3) studying the high-energy behavior of gamma-ray bursts and transients, (4) using high-energy gamma-rays to probe the early universe to  $z \geq 6$ , and (5) probing the nature of dark matter. The LAT is a pair-conversion telescope with a precision tracker and calorimeter, each consisting of a  $4 \times 4$  array of 16 modules, a segmented anticoincidence shield that covers the tracker array, and a programmable trigger and data acquisition system. Each tracker module has 18  $x,y$  tracking planes, consisting of two planes ( $x$  and  $y$ ) of single-sided silicon strip detectors (228  $\mu\text{m}$  pitch) and high- $z$  converter material (tungsten). Each calorimeter module has 96 CsI(Tl) crystals, arranged in an 8 layer hodoscopic configuration with a total depth of 8.5 radiation lengths, giving both longitudinal and transverse information about the energy deposition pattern. The calorimeter's depth and segmentation enable the high-energy reach of the LAT and contribute significantly to background rejection. The overall aspect ratio of the instrument (height/width) is 0.4, allowing a large field-of-view and ensuring that nearly all pair-conversion showers initiated in the tracker will pass into the calorimeter for energy measurement. Data obtained with the LAT will (i) provide rapid notification of high-energy transients, (ii) yield an extensive catalog of several thousand high-energy sources obtained from an all-sky survey, (iii) measure spectra from 20 MeV to more than 50 GeV for several hundred sources, (iv) localize point sources to  $0.3 - 2$  arcmin, (v) map and obtain spectra of extended sources such as SNRs, molecular clouds, and nearby galaxies, and (vi) measure the diffuse isotropic gamma-ray background up to TeV energies.

*Subject headings:* gamma rays: pulsars, AGNs, blazars, SNRs, diffuse ---- instruments: telescopes

## 1. INTRODUCTION

A revolution is underway in our understanding of the high-energy sky. The early SAS-2 (Fichtel, et al 1975) and COS-B (Bignami, et al 1975) missions led to the EGRET instrument (Thompson, et al 1993) on the *Compton Gamma-Ray Observatory*. EGRET performed the first all-sky survey above 50 MeV and made breakthrough observations of high-energy gamma-ray blazars, pulsars, unidentified sources, delayed emission from gamma-ray bursts and solar flares, and diffuse radiation from our Galaxy and beyond, that have all changed our view of the high-energy Universe and raised many new questions. The *Large Area Telescope* (LAT) on the *Gamma-ray Large Area Space Telescope* (GLAST) mission, scheduled for launch by NASA near the end of 2007, offers enormous opportunities for unraveling these mysteries and advancing knowledge in astronomy, astrophysics, and particle physics. The scientific objectives of the LAT include (i) determining the nature of the unidentified sources and the origins of the diffuse emission revealed by EGRET, (ii) understanding the mechanisms of particle acceleration operating in celestial sources, particularly in active galactic nuclei, pulsars, and supernovae remnants, (iii) understanding the high-energy behavior of gamma-ray bursts and transients, (iv) using gamma-ray observations as a probe of dark matter, and (v) using high-energy gamma-rays to probe the early universe to  $z \geq 6$ .

**Commentaire :** Lead: Norris & Omodei

To make significant progress in understanding the high-energy sky, the LAT has good angular resolution for source localization and multi-wavelength studies, high sensitivity over a broad field-of-view to monitor variability and detect transients, good calorimetry over an extended energy band to study spectral breaks and cut-offs, and good calibration and stability for absolute, long term flux measurement.

The LAT, shown in Figure 3.1, is being developed by an international collaboration with primary hardware and software responsibilities at Stanford University, Stanford Linear Accelerator Center, Agenzia Spaziale Italiana, Goddard Space Flight Center, Istituto Nazionale di Fisica Nucleare, Centre National de la Recherche Scientifique / Institut National de Physique Nucléaire et de Physique des Particules, Hiroshima University, Naval Research Laboratory, Royal Institute of Technology, Stockholm, and University of California, Santa Cruz. Other institutions that have made significant contributions to the instrument development include Commissariat à l'Energie Atomique, Institute of Space and Astronautical Science, Ohio State University, Stockholm University, University of Tokyo, Tokyo Institute of Science and Technology, and University of Washington. Table 3.1 summarizes the scientific performance capabilities of the LAT. Details are presented in Section 3.

## 2. SUMMARY OF KEY GLAST LAT SCIENCE OBJECTIVES

The key science objectives addressed by the LAT are largely motivated by the discoveries of EGRET ( $\sim 30$  MeV – 10 GeV) and of ground-based atmospheric Cerenkov telescopes (ACT) above  $\sim 100$  GeV. Because of the combined advances in point spread function (PSF), effective area, energy range, and field of view (FOV), the LAT will have a point-source sensitivity of  $1.6 \times 10^{-9} \text{ cm}^{-2} \text{ s}^{-1}$  ( $E > 100$  MeV) after a 2 year all-sky exposure -- an effective improvement over EGRET by more than a factor of 50. The LAT is designed to explore, with  $\sim 10\%$  spectral resolution, the energy band beyond EGRET's reach and will overlap with ACTs, providing an

absolute calibration. Sources below the EGRET detection threshold ( $\sim 6 \times 10^{-8} \text{cm}^{-2} \text{s}^{-1}$ ) will be localized with subarcminute precision.

## 2.1 *Resolve the Gamma-Ray Sky: The Nature of Unidentified Sources and the Origins of Diffuse Emissions*

The interstellar emission of the Milky Way is an intense celestial background that must be modeled in detail in order to build a reliable source catalog and to determine the galactic gamma ray background (e.g. Hunter, et al; Hartman, et al). It is a major goal of the LAT investigation to accurately determine the sources of interstellar emission from the Milky Way and nearby galaxies. With a reliable gamma-ray background model, we anticipate finding several hundred or more new Galactic sources in addition to the  $\sim 10^4$  expected extragalactic sources (see Figure 2.1). The LAT's angular and energy resolutions will be critical for determining the origin of the unidentified EGRET sources and the new sources discovered in the sky survey.

### 2.1.1 *Unidentified EGRET Sources*

Commentaire : Lead: Reimer

Despite the increase in numbers of unidentified sources from  $\sim 20$  to 170 from COS-B to EGRET, progress toward identification from EGRET observations has been limited because of counterpart confusion in large error boxes, as illustrated in Figure 2.2. The identifications of Geminga and 2CG 342-02 (PSR 1706-44) as pulsars are the lone unambiguous advances. The LAT localizations will be significantly more precise. For example, the Cygnus region, which is very confused for EGRET, even above 1 GeV, will be resolved by the LAT (e.g. see Figure 2.3). As known from the early days of radio, X-ray and IR astronomy, arcminute localizations do enable firm identifications. Many sources are related to star-forming sites in the solar neighborhood or a few kpcs away along the Galactic plane (Gehrels 1999). These sites harbor compact stellar remnants, SNRs and massive stars, i.e., many likely candidate gamma-ray emitters. Evidence exists for a correlation with SNRs (Sturmer & Dermer 1995) as well as OB associations (Romero 1999), reviving the SNOB concept of Montmerle (1979) or making the pulsar option attractive. Pulsar populations can indeed explain a large fraction of unidentified sources close to the Galactic plane (Yadigaroglu & Romani 1997) and possibly in the nearby starburst Gould Belt (Grenier & Perrot 1999). Other candidate objects among the unidentified sources include binary systems, systems with advection-dominated accretion flows onto a black hole, isolated accreting black holes, and Kerr-Newman black holes. The LAT will identify the origin of these sources in three ways:

- (1) Provide excellent source localization (95% confidence diameter) for  $5\sigma$  one-year survey sources and for EGRET sources (Figure 2.2):  $14'$  and  $<0.3'$  respectively, for an  $E^{-2}$  source and  $1^\circ$  and  $1.5'$  respectively, for a source with a spectral cut-off at  $\sim 3$  GeV, as anticipated for pulsars. This will result in an average chance probability of 0.2 and  $7 \times 10^{-5}$ , respectively, for a soft X-ray counterpart; of 0.1 and  $6 \times 10^{-5}$ , resp., for a radio counterpart; and of only  $10^{-2}$  and  $8 \times 10^{-6}$ , respectively, for a radio pulsar counterpart.
- (2) Provide good sensitivity up to 300 GeV, to look for the spectral signature of inverse Compton emission from plerions. Recent studies have indeed found possible associations between X-ray synchrotron nebulae and EGRET sources near the Galactic plane (Roberts & Romani 1998).
- (3) With high sensitivity, large effective area, and good time resolution, look for periodicities on time scales of milliseconds to seconds, typical of ms pulsars, pulsars and binary systems hosting

a neutron star. Extrapolating from EGRET analyses of Geminga (*e.g.*, Mattox 1996), the LAT sensitivity will allow searches in sources as faint as  $\sim 5 \times 10^{-8}$  without a prior knowledge from radio data.

### 2.1.2 *Interstellar Emission from the Milky Way, Nearby Galaxies, and Galaxy Cluster*

**Commentaire** : Lead: Digel

Interstellar emission from the Milky Way is the most prominent feature of the gamma-ray sky. It is matched to Galactic structure scales, such as tangents to the spiral arms and inter-arm regions. A longstanding issue about the Galactic emission is the contribution of unresolved point sources, buried in the highly structured emission at low latitudes. Residuals in the EGRET data (Hunter 1997) above 1 GeV hint at a significant population of unresolved, hard spectrum sources (Pohl 1997). The excellent angular resolution of the LAT above 1 GeV promises great progress in uncovering these sources. The LAT's combination of excellent angular resolution and large effective area will allow the study of external galaxies in the light of their interstellar emission. LAT will resolve the LMC in detail and, in particular, map the massive star-forming region of 30 Doradus (Fig. 2.4). The LAT will also map M31, thereby inaugurating the study of cosmic rays in spiral galaxies other than the Milky Way.

### 2.1.3 *Extragalactic Diffuse Emission*

**Commentaire** : Lead: Moskalenko

An isotropic, apparently extragalactic component of the high energy gamma-ray flux was discovered by SAS-2 and observed by EGRET (Sreekumar 1998). It is well-fitted by a power law spectrum of index -2.1 over the range 30 MeV - 100 GeV. No large-scale spatial anisotropy is seen. Calculations show much of the emission may be produced by unresolved blazars (Stecker & Salamon 1996). However, these calculations require extrapolation of the relative contributions from flaring and quiescent blazar emission. EGRET detects most blazars only during their flaring states, so the quiescent emission is not well measured. The LAT will observe the spectrum with better precision and over a broader energy range than EGRET. Figure 2.5 shows the integral number of photons the LAT will detect versus energy, assuming the flat distribution of Stecker & Salamon. After 5 years, more than 10 million diffuse photons above 100 MeV and more than 1000 above 1 TeV will be collected. The LAT will also directly measure the quiescent (and flaring) emission from thousands of blazars, allowing a detailed calculation of the AGN contribution. After the blazar component has been resolved, any truly diffuse cosmological flux remaining would be of great interest.

## 2.2 *Understand the Mechanisms of Particle Acceleration in Celestial Sources: Active Galactic Nuclei, Pulsars, and Supernovae Remnants*

Gamma-ray observations are a direct probe of particle acceleration mechanisms operating in astrophysical systems. The LAT will explore these systems with >50 times better sensitivity than previous missions. We can anticipate how LAT will advance our knowledge of these non-thermal processes by reference to discoveries made with EGRET in three important source categories: blazars, pulsars, and supernovae remnants.

### 2.2.1 *Blazar AGN Jets*

**Commentaire** : Lead: Lott & Giommi

With its detection of more than 60 AGN, almost all blazars (Hartman 1999), EGRET has strengthened the unified model of AGN as supermassive black holes with accretion disks and jets. Extrapolation of the EGRET LogN-LogS curve, shown in Figure 2.6, using values from

Stecker & Salamon (1996) indicates that the LAT will detect  $\sim 10,000$  AGN in two years. This is more than the number of currently identified blazars. Population studies with this large sample will allow tests of the unified AGN model, studies of jet formation and evolution with redshift, and studies of jet properties with AGN type and orientation. The likely EGRET detection of Cen A (Sreekumar 1999) suggests that other classes of AGN may be detectable. With the LAT's sensitivity and broad energy coverage, quiescent emission and spectral transitions to flaring states can be measured. Figure 2.7 shows how well the LAT will measure AGN spectra.  $\gamma\gamma$  transparency calculations can constrain the bulk Lorentz factors of the outflowing plasma and the location of the acceleration and radiation sites in the inner jet.

For many sources, localizations provided by the LAT will permit high-confidence associations with X-ray, optical and radio counterparts for multiwavelength studies. Magnetic field strength can be estimated from combined X-ray and gamma-ray observations (Catanese 1997). The LAT's wide FOV will allow AGN variability to be monitored on time scales from minutes to years. Flares as bright as that observed by EGRET from 3C 279 (Kniffen 1993) will be measurable with a 2-minute resolution (see Figure 2.8).

### 2.2.2 Pulsars

**Commentaire** : Lead: Romani & Thompson

Electric fields generated by charge depletion along open field lines in pulsar magnetospheres are thought to accelerate particles to  $\sim 10$  GeV and produce the pulsed gamma rays observed by EGRET from at least six isolated neutron stars (Thompson 1997). Because of its large sensitivity and good spatial and spectral resolution at large angles, the LAT will increase this population database by at least an order of magnitude (see Table 2.1) and thereby provide much improved pulsar emission diagnostics: exploring trends between luminosity, period and surface field; gathering large statistics on pulse morphology to constrain beam geometry; searching for periodicities in sources as faint as  $\sim 6 \times 10^{-8} \text{cm}^{-2} \text{s}^{-1}$  to find radio-quiet/gamma-ray-loud pulsars (i.e., Geminga-like neutron stars). As shown in Table 2.1, very different numbers of radio-selected and radio-quiet gamma-ray pulsars are predicted depending on whether the acceleration site resides near the polar cap or close to the light cylinder (outer gap). This is because of the very different gamma-ray beam patterns in the two models. The LAT will definitely test these predictions and provide a pulsar sample independent of radio selection. The increased sensitivity at high energies will also allow detection of older pulsars, intrinsically fainter, but with harder spectra, which could not be detected by EGRET. The good energy resolution of LAT over a broad energy range will allow measurements of the shapes of pulsar spectral cutoffs. Cutoffs, generally well above 1 GeV, relate to the surface magnetic field strength and provide another discriminator between polar cap (e.g., Daugherty & Harding 1996) and outer gap models (e.g., Romani 1996). The LAT data will augment spectral modeling of pulsed emission from X-rays through gamma-rays and constrain the primary radiation and pair creation mechanisms initiating the particle cascades. In particular, phase resolved spectral index variations will tighten the constraints on model parameters and distinguish between 1- and 2-pole geometries.

**Commentaire** : Lead: Romani

### 2.2.3 Supernova Remnants and Cosmic Rays

Cosmic rays with energy less than  $10^{15}$  eV have long been thought to be shock-accelerated in supernova remnants (SNRs). Recent X-ray and TeV observations have confirmed electron acceleration up to TeV energies by detecting non-thermal bremsstrahlung and inverse Compton emission from a few SNR shells, in particular from plerions (e.g., Tanimori 1998, Koyama

1995). Freshly accelerated protons have not yet been detected through their  $\pi^0$  decay spectral signature however. EGRET disproved a metagalactic origin of the cosmic rays (Sreekumar 1992; 1993) and found gamma-ray sources toward a few remnants, but its angular resolution would not allow a firm identification. The LAT's excellent spatial and energy resolutions will separate the extended shell emission of an SNR from a compact source (pulsar, tiny plerion) inside it. It will also spectrally resolve electron and nuclei emission. The LAT will resolve >10 remnants, to establish the location of cosmic ray production. In  $\gamma$  Cygni for example, the central source, coincident with an X-ray source, is suspected to be a pulsar (Brazier 1996). In the simulation shown in Figure 2.8, the EGRET flux was partitioned between the pulsar and a shell segment. The pulsar components can be clearly distinguished from the shell.

### 2.3 Study the High Energy Behavior of Gamma-Ray Bursts and Transients

**Commentaire :** Lead: Norris & Omodei

There have been recent breakthroughs in our understanding of gamma-ray bursts (GRBs) with the discovery of X-ray, optical, and radio afterglows, and delayed high-energy gamma-ray emission. We now know that GRBs are cosmological and involve extremely powerful, relativistic explosions. What triggers the explosions is not known, but theories suggest that GRBs are signatures of black hole creation and tracers of star formation at early epochs. It is thought that an initial fireball creates a super-relativistic blast wave resulting in an afterglow that cascades down from gamma-rays to radio. EGRET detected two components of high energy gamma-ray emission from GRBs: prompt emission, well defined at lower energies, and a delayed component extending to GeV energies that lasted more than an hour in the case of GRB940217 (Hurley 1994). The initial pulsed component was poorly measured by EGRET because of its severe spark chamber dead time ( $\sim 100$  ms/event). The LAT is designed with low deadtime ( $\sim 20$   $\mu$ s/event) so that even a high-flux burst like GRB940217 will be detected with very little (< few %) dead time during the most intense part of the burst. Figure 2.9 shows the distribution of times between photon detections, for a relatively bright burst with fluence of 2000 photons ( $E > 10$  MeV), assuming that pulse widths scale as  $\sim E^{-0.3}$ , extrapolated from BATSE (Norris 1999). For reference, the EGRET dead time is indicated in the figure, showing the dramatic improvement the LAT provides for high energy burst science. The delayed component of GRBs will also be much better measured because of LAT's increased effective area, larger FOV, and low self-veto at >GeV energies. Models of delayed GeV emission, for example, involving production of gamma-rays from ultra-high-energy cosmic rays (Bottcher & Dermer 1998) and interaction with the intergalactic medium (Plaga 1995), can be tested. Internal and external shock models are currently constrained primarily by spectral and temporal behavior at BATSE energies (Fenimore & Ramirez-Ruiz 1999). The LAT's sensitivity will force comparison of models with observations over a dynamic range in energy  $\sim 10^3$ - $10^4$ , instead of the factor of  $\sim 20$  afforded by BATSE. The LAT will provide spectral diagnostics of bright bursts and can measure exponential high energy spectral cutoffs expected from moderately high redshift GRBs caused by  $\gamma\gamma$  absorption in the cosmic infrared background (complementing AGN probes). LAT will distinguish such attenuation from  $\gamma\gamma$  absorption internal to the sources. Internal absorption is expected to produce time-variable breaks in power-law energy spectra. Signatures of internal absorption will constrain the bulk Lorentz factor and adiabatic/radiative behavior of the GRB blast wave as a function of time (Baring 1999). Detailed simulations show that the LAT will detect  $\sim 200$  GRBs per year,  $\sim 40$  times as many as EGRET detected during the entire CGRO mission (Table 2.2). More speculatively, simulations show that the LAT could make major discoveries in quantum gravity by detecting an energy-dependent dispersion of light

from GRB (Amelino-Camelia 1998). The LAT properties important for this measurement are its broad energy range, sensitivity at high energies, and good timing. The LAT's low deadtime and simple event reconstruction, even for multi-photon events, will enable searches for evaporation of primordial black holes.

Simulations show that for ~25% of the bursts, LAT localizations are sufficient for direct optical counterpart searches. For these ~50 GRBs per year, LAT will rapidly calculate the absolute position onboard. The information will then be sent to the ground via the real-time TDRSS link and distributed on the GCN network, within ~15 seconds. Fainter high-energy bursts will be detected by subsequent ground analysis.

#### 2.4 Probe Dark Matter

Commentaire :

The rotation curves of galaxies, structure-formation arguments, and the dynamics and weak lensing of clusters of galaxies all provide strong evidence for the existence of a vast amount of dark matter in the Universe, particularly in galactic halos. The LAT will make important measurements relevant to the search for dark matter. Baryonic dark matter in the Milky Way may exist in cold molecular clouds (e.g., Sciama 1999; De Paolis 1999). Its signature would be a hardening of the interstellar gamma-ray spectrum above ~1 GeV. Such an excess can be measured by the LAT, with its excellent background rejection and sensitivity. The fine angular resolution will allow precise measurements of the molecular gas emissivity at the periphery of the Milky Way, to set limits on baryonic dark matter (Digel 1996). Narrow gamma-ray annihilation lines would be a definitive signature of nonbaryonic dark matter (WIMPs) and would determine the WIMP mass. Calculations from SUSY models show that a window exists for the LAT to discover this exotic matter (Ullio & Bergström 1998) beyond the reach of accelerator and energetic neutrino searches. (e.g., Wells 1998). For photons incident at  $> 50^\circ$ , LAT will have ~4% energy resolution, allowing a sensitive search for WIMP annihilation lines. Figure 2.10 shows the 95% CLUL for detection of such lines by the LAT, observing a 1 sr cone surrounding the Galactic Center after a five year all-sky survey. Overplotted on the figure for comparison are two types of SUSY models (Ullio 1999). Both  $\chi\chi \rightarrow \gamma\gamma$  and  $\chi\chi \rightarrow \gamma Z$  final states are expected. The two narrow photon lines from these states are separable provided the mass of the lightest SUSY particle  $M_\chi < M_Z/\sqrt{(4\Delta E/E)}$ , or  $M_\chi < 230$  GeV for 4% energy resolution.

#### 2.5 Use high-energy gamma-rays to probe the early universe to $z \geq 6$

Photons above 10 GeV can probe the era of galaxy formation through absorption by near UV, optical, and near IR extragalactic background light (EBL). The latter depends sensitively on star formation rates and the presence of dust (Stecker 1992; Madau & Phinney 1996; MacMinn & Primack 1996). Too few sources have been detected so far to separate intrinsic turnovers from EBL absorption effects.

With as many as  $10^4$  AGN detectable up to  $z \geq 6$  (Figure 2.1), the LAT data will yield conclusive results (Salamon & Stecker 1998, Chen & Ritz 1999). Spectra to more than 50 GeV can be determined for several hundred sources. The ratio of integrated flux above 10 GeV to that above 1 GeV as a function of redshift is shown in Figure 2.11 for one EBL absorption model (Stecker 1999). The large number of detected blazars over a broad energy range will provide the data necessary to evaluate the gamma-ray optical depth as a function of redshift and energy, and will mitigate peculiar effects of individual sources.

### 3. LARGE AREA TELESCOPE

The LAT is designed to measure the direction and energy of gamma-rays incident over a wide field-of-view (FOV), while rejecting background from cosmic rays. The design approach that resulted in the instrument described in detail in Section 3.1, first and foremost, made extensive use of detailed simulations of the detector response to signal (celestial gamma-rays) and backgrounds (cosmic rays, albedo gamma-rays, etc.). Second, detector technologies were chosen that have an extensive history of application in space-science and high-energy physics with demonstrated high reliability. Third, relevant test models were built to demonstrate critical requirements, such as power, efficiency, and detector noise occupancy, could be readily met. Fourth, these detector-system models, including all subsystems, were studied in accelerator test beams to validate the design and the Monte Carlo programs used in the simulations (Atwood et al. 1999).

Finally, the modular design of the LAT allowed the construction, at reasonable cost, of a full-scale, fully functional engineering demonstration telescope module for validation of the design concept and technology, including mass, power, and noise budgets. This engineering model was also successfully flown on a high-altitude balloon to demonstrate system level performance in a realistic, harsh background environment (REFERENCE).

#### 3.1 *Technical Description*

The LAT, illustrated in Figure 3.1, is a pair-conversion telescope with a precision converter-tracker and calorimeter, each consisting of a  $4 \times 4$  array of 16 modules supported by a low-mass Grid structure. A segmented anticoincidence detector shield covers the tracker array, and a programmable trigger and data acquisition system (DAQ) utilizes prompt signals available from the tracker, calorimeter, and anticoincidence detector subsystems to form a trigger. Upon triggering, the DAQ initiates the read out of these three subsystems and utilizes on-board event processing to reduce the rate of events transmitted to the ground to a rate compatible with the downlink available to the LAT (1 Mbps, orbit-average). The on-board processing is optimized for rejecting events triggered by cosmic-ray background particles while maximizing the number of events triggered by gamma-rays that are transmitted to the ground. Heat produced by the tracker, calorimeter, and DAQ electronics is conducted outward to radiators through constant-conductance heat pipes in the Grid.

##### 3.1.1 *Precision converter-tracker*

Each tracker module has 18  $x,y$  tracking planes, consisting of two planes ( $x$  and  $y$ ) of single-sided silicon strip detectors (AC-coupled, 400  $\mu\text{m}$  thick, 228  $\mu\text{m}$  pitch) and high- $z$  converter material (tungsten). Figure 3.2 illustrates schematically a single  $x$  or  $y$  layer.

The support structure for the detectors and converter foils is composed of a stack of 19 composite panels, call “trays,” aligned at the four corners and held in compression by cables threaded through the corners. Sidewalls provide additional strength, protect the electronics, and conduct heat to the TKR base. The tray structure is a low-mass carbon-composite assembly composed of a closeout, face sheets, and vented honeycomb core. Carbon-composite is chosen for its long radiation length, high modulus-to-density ratio, and thermal stability.

The tray panel structure is about 3 cm thick and is instrumented with converters, detectors, and front-end electronics. All trays are nearly identical in construction, although the top and bottom ones are special, as they include mechanical interfaces to the Grid and ACD and have detectors on only one face. Figure 3.3 shows a flight tracker tray.

An  $x,y$  measurement plane consists of a “ $y$ ” layer of detectors on the bottom of one tray together with the “ $x$ ” detector layer on the top of the tray just below, with only a 2-mm separation. The converter layer lies immediately above the “ $y$ ” layer. There are 16  $x,y$  planes at the top of the tracker with converters. The last two  $x,y$  planes have no converter foils.

Incident photons preferentially convert in one of the converters, and the resulting  $e^-$  and  $e^+$  particles are tracked by the silicon-strip detectors (SSDs) through successive planes. The pair conversion signature is also used to help reject the much larger background of charged cosmic rays. The high intrinsic efficiency and reliability of this technology enables straightforward event reconstruction and an excellent PSF with small tails. The tracker design emphasizes the importance of an outstanding single-photon point spread function (PSF) at high as well as low energy. The tracker angular resolution is determined by the ratio of the detector resolution to the lever arm over which the measurement is made. The lever arm is restricted at high energy by the need for a large field-of-view (FOV) and by the fact that the direction measurement must be made before the first bremsstrahlung photon is emitted, *i.e.* before the electron has passed through  $\sim 1$  radiation length of material. The LAT design emphasizes the high efficiency ( $>99\%$ ) and excellent position resolution obtainable from silicon strip detectors. These detectors also have fine two-hit resolution which enhances the track reconstruction capabilities.

Pair conversion trackers contain far more material than would normally be put into a particle tracking device. Multiple scattering and bremsstrahlung production severely limit the obtainable resolution. To get optimal results requires that the electron and positron directions be measured immediately following the conversion. At 100 MeV the penalty for missing one of the first hits is about a factor of 2 in resolution, resulting in large tails in the PSF. Figure 3.4 illustrates these and other considerations in tracker design that impact the PSF. In particular, it is important that the silicon-strip detector layers have high efficiency, are held close to the converter foils, the inactive regions are localized and minimized, and the passive material is minimized.

One of the most complex LAT design trades was the balance between the need for thin converters, to achieve a good PSF at low energy, where the PSF is determined primarily by the  $1/E$  dependence of multiple scattering, versus the need to increase converter material to maximize the effective area, important at high energy. It was found that the overall science performance is best when the tracker is divided into two regions, “front” and “back.” The front region (first 12  $x,y$  tracking planes) has thin converters, each 0.03 radiation lengths thick, to optimize the PSF at low energy, while the converters in the back (4  $x,y$  planes after the front tracker section) are 7 times thicker, to maximize the effective area at the expense of less than a factor of two in angular resolution (at 1 GeV) for photons converting in that region. Instrument simulations show that the LAT point source sensitivity is approximately balanced between the front and back tracker sections.

Note that the thick “back” converter planes work well only with nearly 100% efficient detectors. Because of the large multiple scattering at low energies the photon direction must be measured accurately in the first two detector planes following the conversion.

### 3.1.2 *Calorimeter*

Each calorimeter module has 96 CsI(Tl) crystals, arranged in an 8 layer hodoscopic configuration with a depth of 8.5 radiation lengths (for a total instrument depth of 10.1 radiation lengths), giving both longitudinal and transverse information about the energy deposition pattern. Each crystal element is read out by PIN diodes. The calorimeter's depth and segmentation enable the high-energy reach of the LAT and contribute significantly to background rejection. In particular, the energy resolution at high energies is achieved through the application of shower leakage corrections.

### 3.1.3 *Anticoincidence Detector*

The ACD array of plastic scintillator tiles provides much of the rejection of charged particle backgrounds. Its segmentation avoids the "backsplash" self-veto that affected EGRET above a few GeV. Each ACD tile is read out by waveshifting fibers, embedded in the tile, connected to redundant photomultiplier tubes.

### 3.1.4 *Data Acquisition System (DAQ)*

This system collects the data from the subsystems, implements the multi-level event trigger, and provides an on-board science analysis platform to search for transients.

### 3.2 *Instrument Operations*

### 3.3 *Instrument Modeling*

### 3.4 *Background Rejection*

#### 3.4.1 *Background Model*

#### 3.4.2 *Background Rejection*

### 3.5 *Telescope Performance – Calibration*

### 3.6 *Observing Strategy*

### 3.7 *LAT Data Processing and Data Products*

#### 3.7.1 *Transient Alerts*

#### 3.7.2 *Source Monitoring*

#### 3.7.3 *Catalog*

#### 3.7.4 *Diffuse Model*

#### 3.7.5 *Level-1 Data*

## 4. SUMMARY

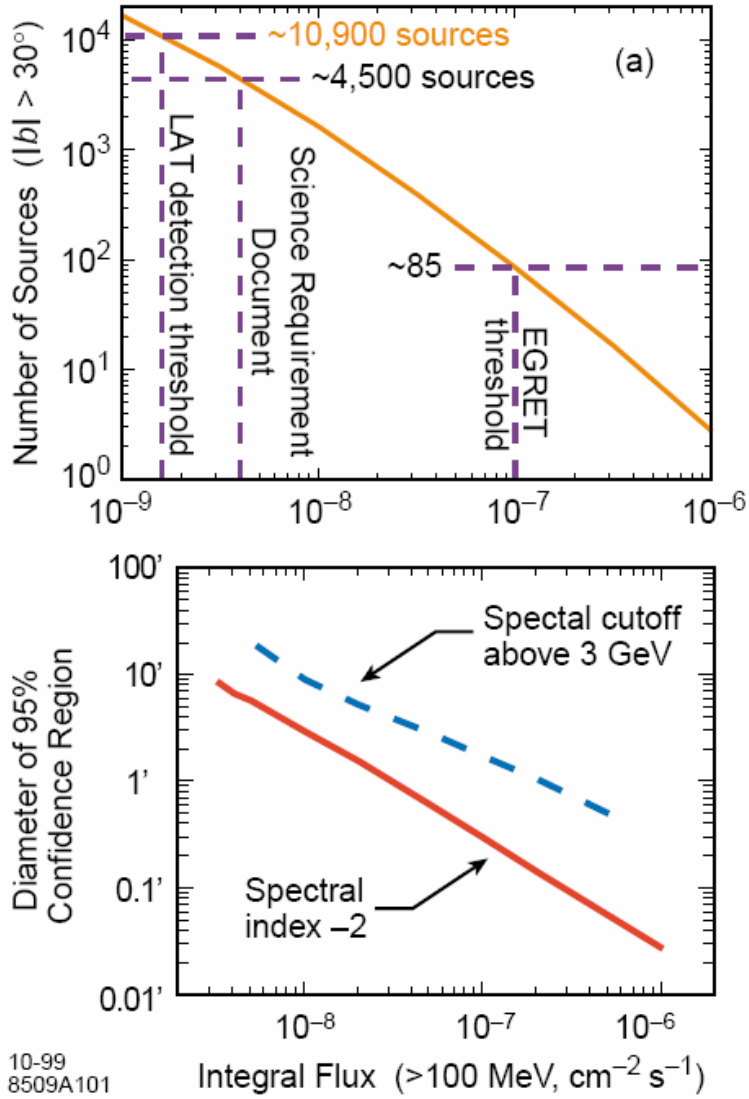


Figure 2.1: (a) The expected number of AGN detected with LAT at  $|b| > 30^\circ$  and, (b) one year, all sky-survey source localization capability. (Note: s/c systematics will limit capability to  $\geq .3'$ ).

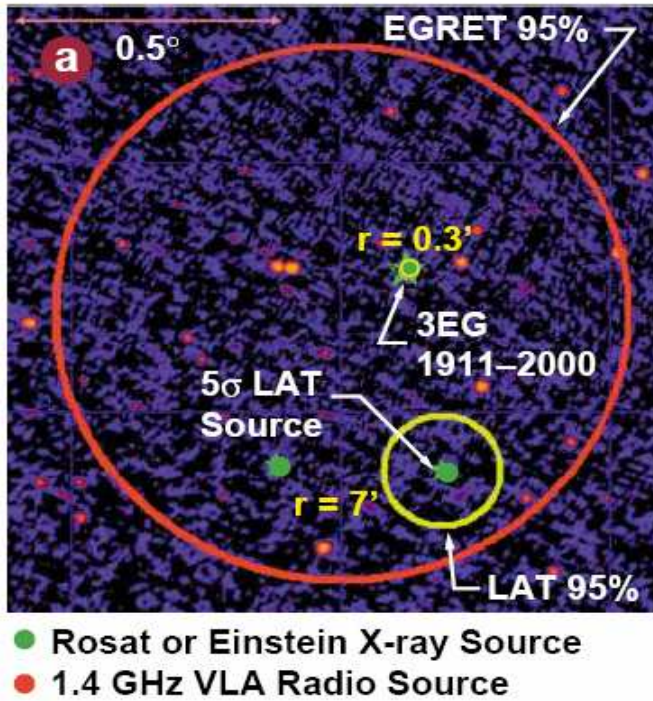


Figure 2.2: LAT 95% confidence radii localizations of a  $5\sigma$  source in the one-year sky survey and of the EGRET source 3EG 1911-2000 compared with the EGRET localization.

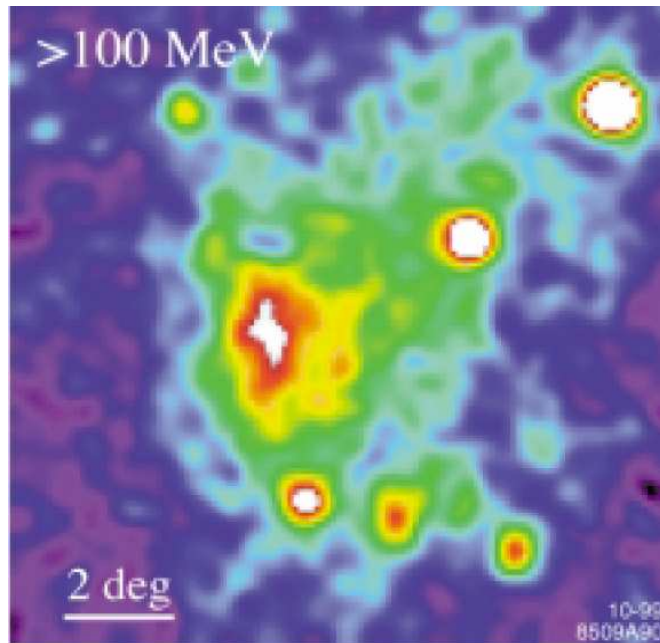


Figure 2.4: Simulated map of the interstellar emission from the LMC observed in a 2-year sky survey with the LAT. The simulation is based on a model of the interstellar emission in the LMC by Sreekumar (1999).

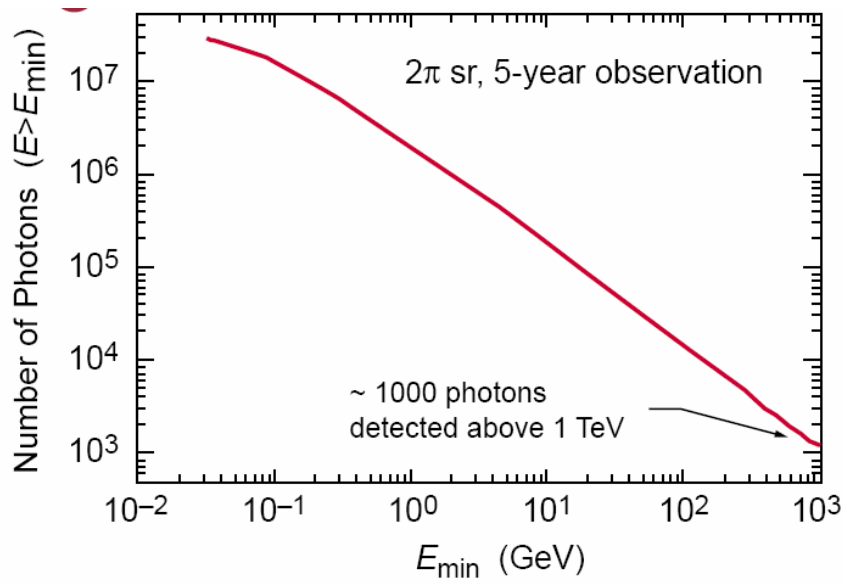


Figure 2.5: Expected number of diffuse extragalactic photons detected by the LAT after 5 years, based on the model of Stecker and Salamon (1996).

Figure 2.6: Extrapolation of EGRET  $\text{Log}N - \text{Log}S$  curve, suggesting that the LAT will detect as many as  $\sim 10^4$  extragalactic sources in two years.

Figure 2.7: Estimated LAT measurement of AGN spectra.

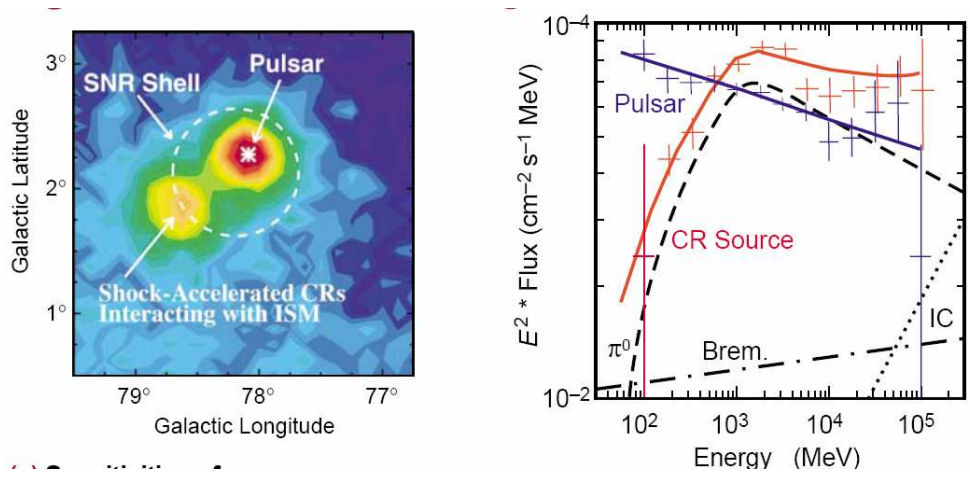


Figure 2.8: Simulation showing the ability of the LAT to spatially and spectrally resolve the SNR  $\gamma$ -Cygni.

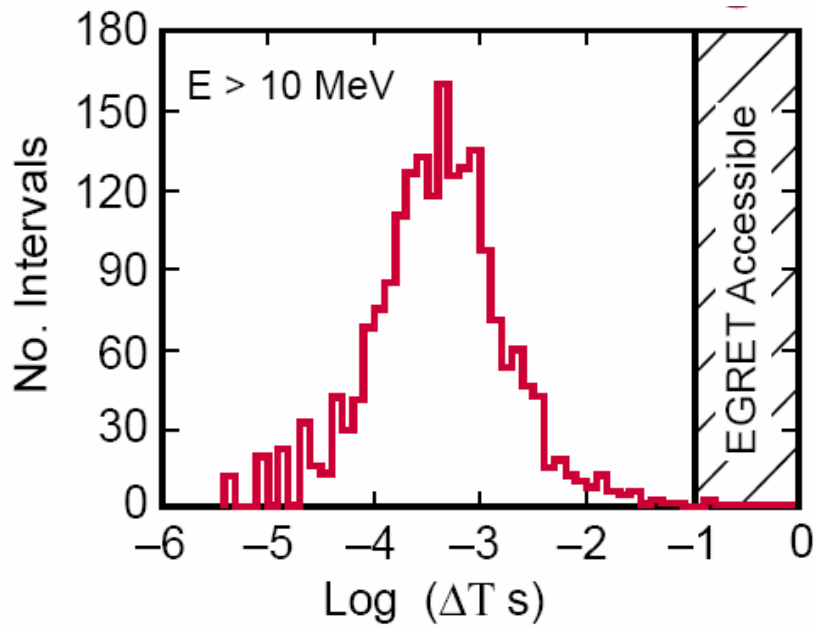


Figure 2.9: Simulated distribution of times between LAT photon detections from the 20<sup>th</sup> brightest burst expected in one year.

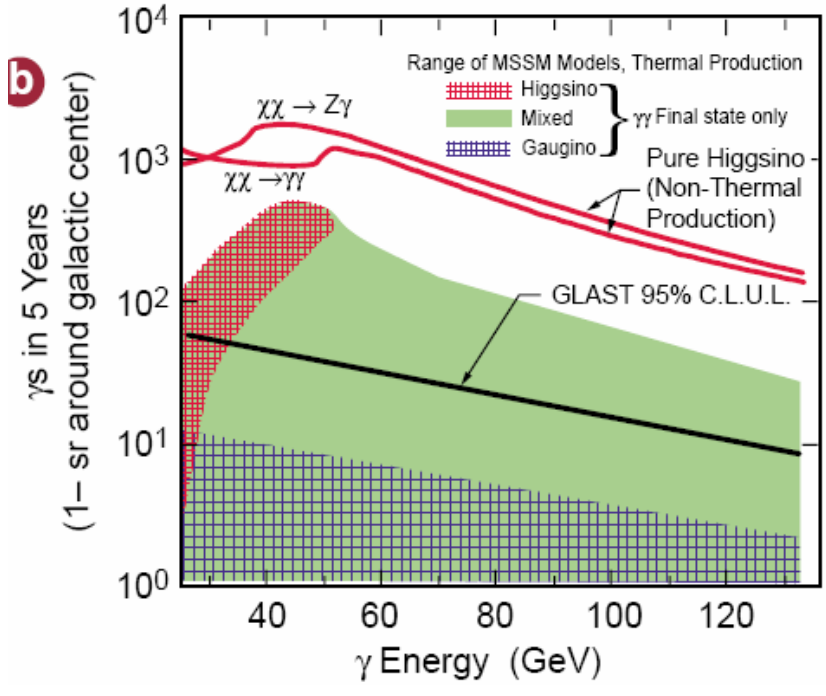


Figure 2.10: GLAST LAT monoenergetic  $\gamma$ -ray line sensitivity (95% confidence level upper limit) as a function of  $\gamma$ -ray energy. Colored areas are a range of MSSMs within a restricted parameter space from standard assumptions and thermal relic abundance calculations. Red lines are assuming a non-thermal origin with Higgsinos accounting for the bulk of the Galactic halo.

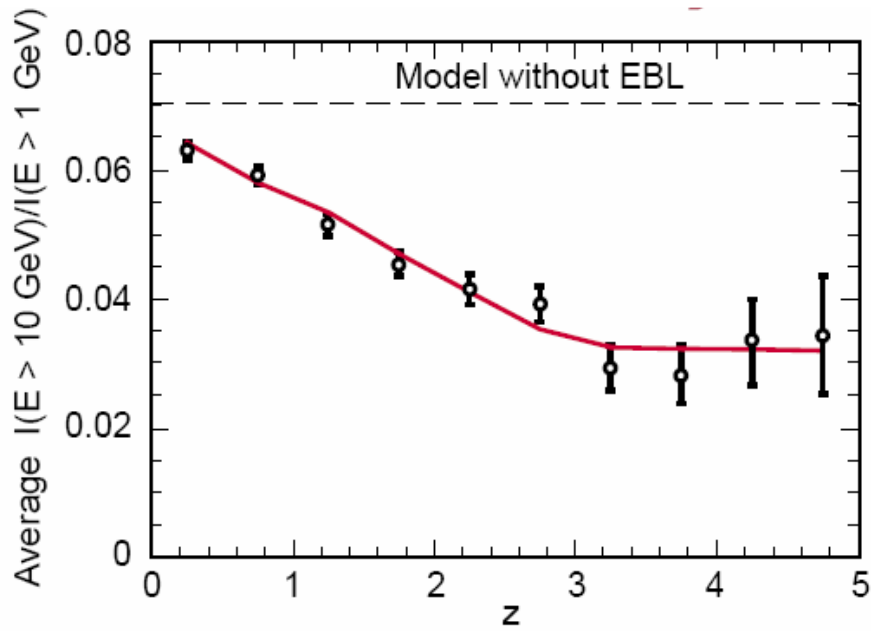


Figure 2.11: LAT probes optical-UV Extragalactic Background Light by measurement of high-energy spectral roll offs of AGN: Shown is a simulation of the ratio of integrated flux above 10 GeV to that above 1 GeV as function of redshift for the EBL absorption model of Stecker et al. (1999).

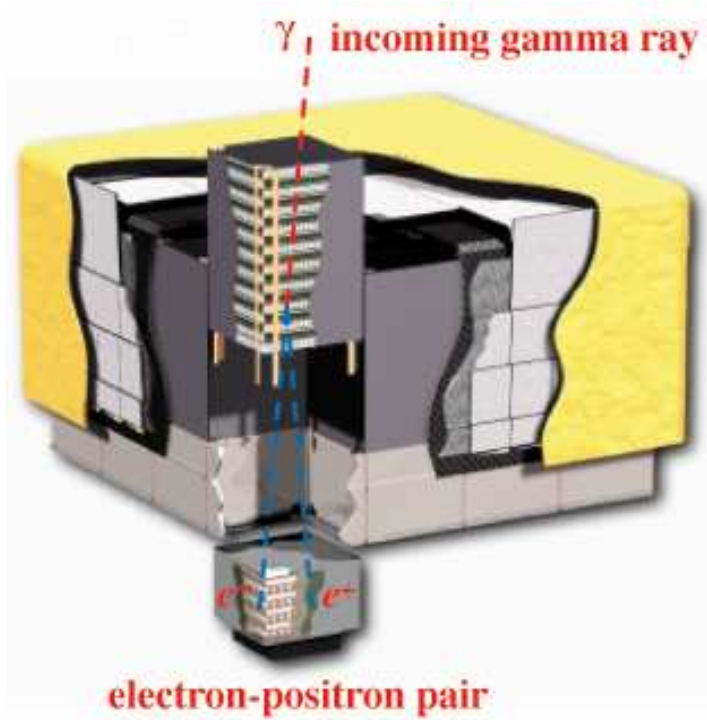


Figure 3.1: Schematic of the Large Area Telescope

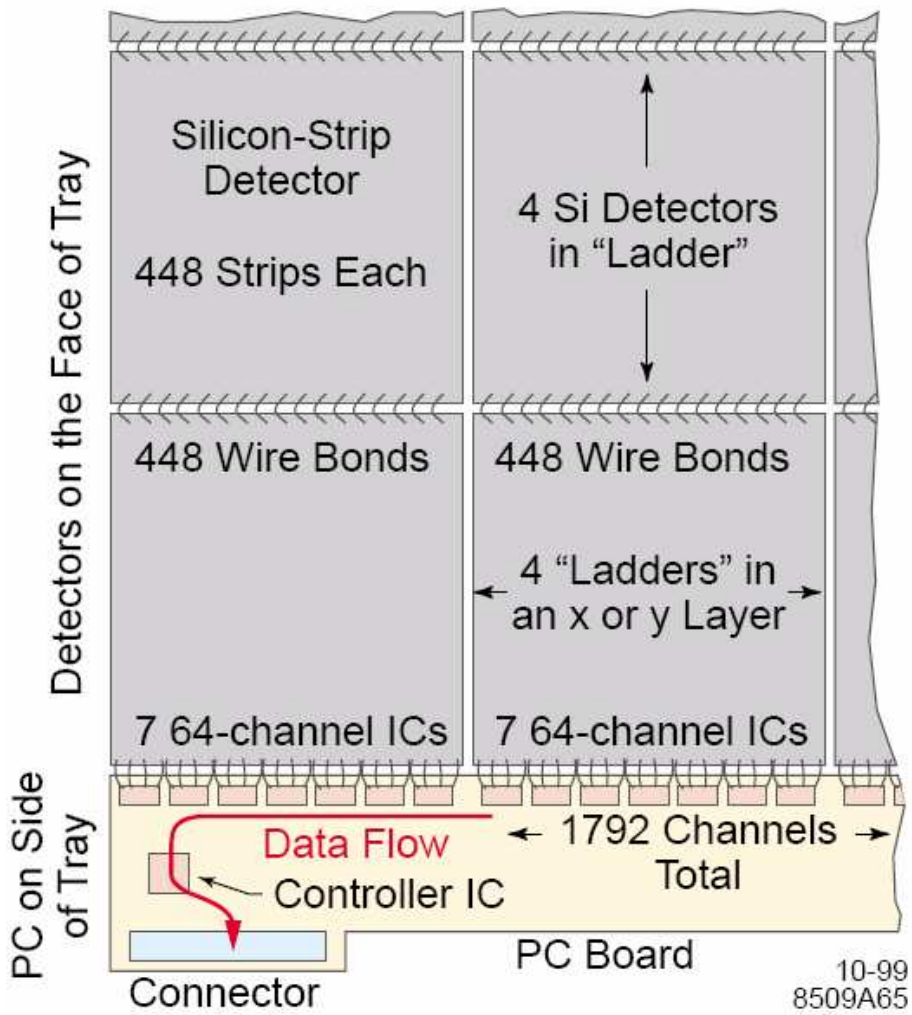


Figure 3.2: Schematic depiction of roughly 1/4 of a tracker detector layer, x or y (not to scale).

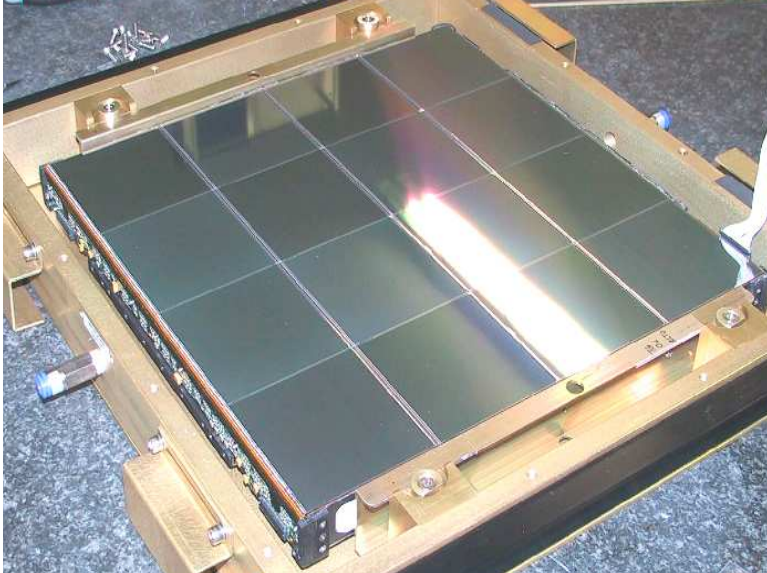


Figure 3.3: A flight tracker tray.

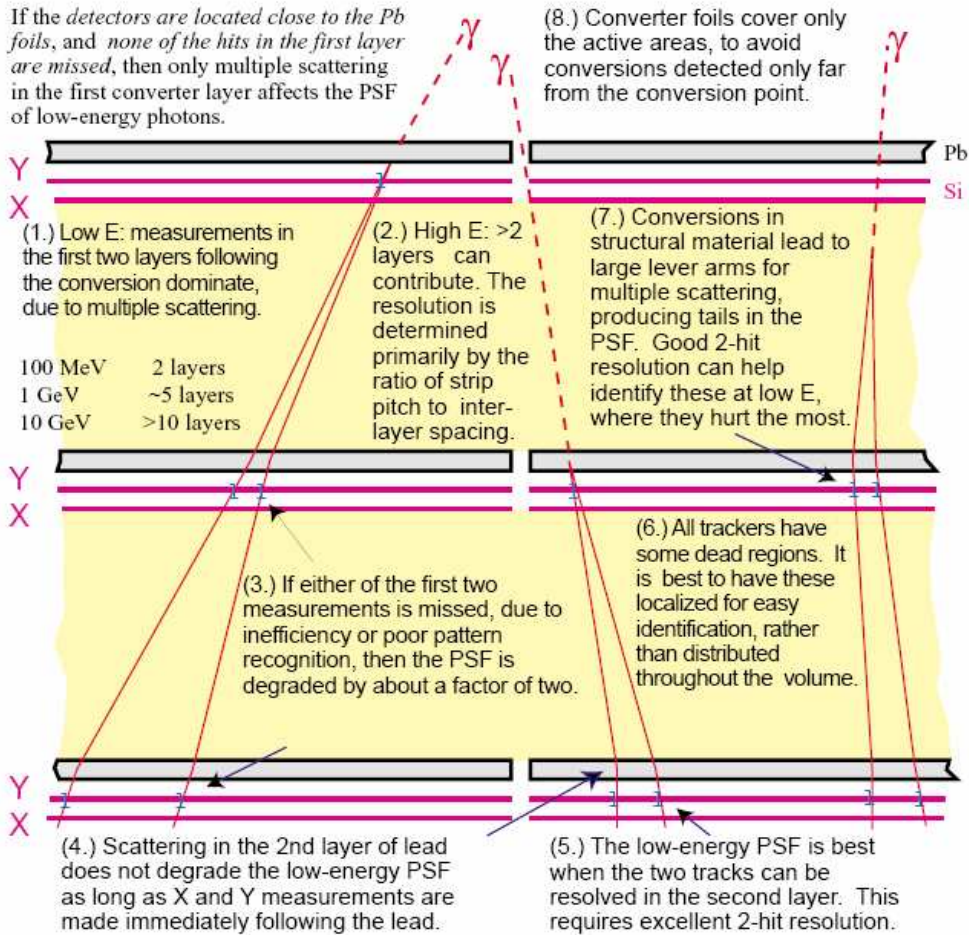


Figure 3.3: Qualitative illustration of how the design of the pair-conversion telescope tracker impacts the quality of the PSF. (Not to scale)

TABLE 2.1

ESTIMATED NUMBER OF DETECTABLE PULSARS FOR THE POLAR CAP AND OUTER GAP MODELS

Pulsar type	EGRET detections	LAT / polar cap	LAT / outer gap
Radio	7	150	50
Millisecond	1	20	-
Radio quiet	1	<10	600

TABLE 2.2

ESTIMATED NUMBER OF GRBS AND AFTERGLOWS DETECTED BY THE LAT

Instrument	GRBs	Afterglows
EGRET	6	2-3
GLAST LAT	200-250	60-120

TABLE 3.1  
SUMMARY OF *LARGE AREA TELESCOPE* INSTRUMENT PERFORMANCE

TABLE 3.2  
KEY LAT TRACKER PARAMETERS

Parameter	Value	Performance Drivers and Constraints
Noise occupancy (fraction of channels with noise hits per trigger)	$10^{-6}$	Trigger rate, data volume, track reconstruction. The requirement, driven by the trigger rate, is $<10^{-4}$
Single channel efficiency for minimum ionizing particle (MIP), within fiducial volume	$> 99\%$	PSF, especially at low energy. It is important to measure the tracks in the first 2 planes following the conversion point.
Ratio of strip pitch to vertical spacing between tracker planes	0.0064	High-energy ( $> 1$ GeV) PSF
Silicon-strip detector pitch (center-to-center distance between strips)	228 $\mu\text{m}$	Small value needed to maintain a small pitch-to-plane-spacing ratio without destroying the FOV.
Aspect ratio (Height/Width)	0.4	Large FOV for photons with energy determination
Front converter foil thickness (radiation lengths)	$12 \times 0.03$	Minimize thickness per plane for low-energy PSF, but not so much that support material dominates. Maximize total thickness to maximize effective area.
Back converter foil thickness (radiation lengths)	$4 \times 0.20$	Effective area and FOV at high energies
Support material and detector material per XY plane (radiation lengths)	0.013	Stable mechanical support is needed, but much of this material is in a non-optimal location for the PSF. Minimize to limit PSF tails from conversions occurring in support material.

TABLE 3.3  
KEY LAT CALORIMATER PARAMETERS

Parameter	Value	Performance Drivers and Constraints	
Depth, including tracker (radiation lengths)	10.1		Trigger rate, data volume, track reconstruction. The requirement, driven by the trigger rate, is $<10^{-4}$
Sampling (angle dependent)	> 90% active	Energy resolution	PSF, especially at low energy. It is important to measure the tracks in the first 2 planes following the conversion point.
Longitudinal segmentation	8 segments		High-energy ( $> 1$ GeV) PSF
Lateral segmentation	~1 Moliere radius		Small value needed to maintain a small pitch-to-plane-spacing ratio without destroying the FOV.

TABLE 3.4  
KEY LAT ANTICOIDENCE DETECTOR PARAMETERS

Parameter	Value	Performance Drivers and Constraints
Segmentation into tiles	< 1000 cm <sup>2</sup> each	Minimize self-veto, especially at high energy. This value is for the top. Side tiles are smaller, to achieve a similar solid angle, as seen from the calorimeter.
Efficiency of a tile for detecting a MIP	> 0.9997	Cosmic ray rejection, to meet a requirement of 0.99999 when combined with the other subsystems.
Number of layers	1	Minimize material, mass, and power. Dual readout on each tile for redundancy.
Micrometeroid / thermal blanket thickness (gm cm <sup>2</sup> )	<XXX	Small value needed to minimize gamma-ray production in this passive material from cosmic-ray interactions.